The Zonal Dimension of the Indian Ocean Meridional Overturning Circulation

SYBREN S. DRIJFHOUT

Royal Netherlands Meteorological Institute (KNMI), De Bilt, Netherlands

ALBERTO C. NAVEIRA GARABATO

National Oceanography Centre, Southampton, Southampton, United Kingdom

(Manuscript received 5 June 2006, in final form 9 May 2007)

ABSTRACT

The three-dimensional structure of the meridional overturning circulation (MOC) in the deep Indian Ocean is investigated with an eddy-permitting ocean model. The amplitude of the modeled deep Indian Ocean MOC is 5.6 Sv (1 Sv $\equiv 10^6$ m^3 s^{-1}), a broadly realistic but somewhat weak overturning. Although the model parameterization of diapycnal mixing is inaccurate, the model's short spinup allows the effective diapycnal velocity (the sum of model drift and the explicitly modeled diapycnal velocity) to resemble the true, real-ocean diapycnal velocity. For this reason, the model is able to recover the broad zonal asymmetry in the turbulent buoyancy flux that is suggested by observations. The model features a substantial deep, depth-reversing zonal circulation of nearly 50% of the MOC. The existence of this circulation, brought about by the zonally asymmetric distribution of diapycnal mixing, implies a much slower ventilation of the deep Indian Ocean (by a factor of 5–6) than would be in place without zonal interbasin exchanges. It is concluded that the zonal asymmetry in the distribution of diapycnal mixing must have a major impact on the deep Indian Ocean's capacity to store and transform climatically significant physical and biogeochemical tracers.

1. Introduction

The Indian Ocean is thought to be a key region in the global overturning circulation despite hosting no significant deep-water production. As illustrated, for example, by Schmitz (1995), O(10 Sv) (1 Sv $\equiv 10^6$ m^3 s^{-1}) of Circumpolar Deep Water (CDW) from the Southern Ocean may be transformed to less dense deep and intermediate waters in the Indian Ocean, a lightening that mediates what is perhaps the most important form of North Atlantic Deep Water (NADW) compensation via interbasin exchange. Intense deep upwelling and mixing in the Indian Ocean are also highlighted by Ganachaud and Wunsch (2000). In their inverse analysis of the global ocean circulation, basin-averaged dia-neutral velocities and diffusivities in the Indian Ocean bottom layers are larger than anywhere else in the world and are associated with the upwelling of 11 ± 5

Sv across the γ^n = 28.11 kg m^{-3} surface, which is embedded in the CDW and NADW density classes [γ^n is the neutral density of Jackett and McDougall (1997)].

Owing to the Indian Ocean's key status in the global problem, numerous attempts have been made to estimate its meridional overturning circulation (MOC). Nonetheless, significant disagreements between the various estimates of the Indian Ocean MOC's strength and vertical structure remain. For example, estimates of the deep overturning across the southern boundary of the Indian Ocean based on the analysis of hydrographic transect and current meter data include values as different as 12 ± 3 (Robbins and Toole 1997), 17 ± 5 (Macdonald 1998), 11 ± 4 (Ganachaud et al. 2000), 10.1 (Bryden and Beal 2001), 23 ± 3 (Sloyan and Rintoul 2001), 18 (Talley et al. 2003), and 9.2 ± 2.7 Sv (Lumpkin and Speer 2007). Further, a marked discrepancy exists between these estimates and results from ocean general circulation models (OGCMs), which exhibit a much weaker overturning [e.g., 2 (Lee and Marotzke 1997; Zhang and Marotzke 1999) and 3 Sv (Garternicht and Schott 1997)]. The only exception is the model of Ferron and Marotzke (2003), which obtains a deep In-

Corresponding author address: S. S. Drijfhout, Royal Netherlands Meteorological Institute (KNMI), P.O. Box 201, 3730 AE De Bilt, Netherlands.
E-mail: drijfhou@knmi.nl

dian Ocean overturning of 17 Sv by assimilating hydrographic sections with a 4D variational method. In turn, a radiocarbon budget of the deep Indian Ocean yields an intermediate overturning magnitude of 8.2 ± 1.5 Sv (Srinivasan et al. 2000).

The discrepancy between modeling and observational studies is generally attributed to the excessively weak deep vertical mixing prescribed in OGCMs; ocean models typically use a constant vertical diffusivity of 10^{-4} $m^2\,s^{-1}$, whereas Ganachaud and Wunsch (2000) estimate the basin-averaged dianeutral diffusivity in the Indian Ocean to be up to 12 times larger in the deepest layers. The existence of a causal link between unrealistically low vertical mixing rates and the weak deep overturning in model simulations of the Indian Ocean has been substantiated recently (Palmer et al. 2007). On the other hand, several of the deep overturning estimates from observational studies appear to imply that a surprisingly large fraction of the turbulent kinetic energy dissipation required to maintain the abyssal stratification of the global ocean takes place in the Indian Ocean. For instance, sustaining the overturning of 23 ± 3 Sv estimated by Sloyan and Rintoul (2001) calls for O(1.5 TW) to be dissipated in the deep Indian Ocean (Naveira Garabato et al. 2005), a value that may exceed one-half of the net turbulent kinetic energy dissipation associated with diapycnal mixing in the global deep ocean (Wunsch and Ferrari 2004).

Perhaps because of this persistent difficulty in determining the Indian Ocean MOC, another major feature of the deep regional circulation is often overlooked. This feature stems from the marked zonal asymmetry in the topographic complexity of the Indian Ocean, which translates into a similar asymmetry in the rate of tidal energy dissipation—tidal energy is dissipated far more efficiently in the western than in the eastern Indian Ocean (Egbert and Ray 2001), assuming that scattering of the barotropic tide to higher modes is a good proxy for dissipation. Given that tides provide one of the two major energy sources for diapycnal mixing in the deep ocean (Wunsch and Ferrari 2004), we may then expect that a zonal asymmetry should also be apparent in the intensity of diapycnal mixing. This expectation is confirmed by a map of in situ estimates of the middepth turbulent buoyancy flux induced by internal wave breaking (Fig. 1), obtained from the application of an internal wave–wave interaction model to CTD/lowered ADCP (LADCP) measurements of density and velocity fine structure [Naveira Garabato et al. (2005); see Kunze et al. (2006) for a detailed description of the estimation technique].

The western intensification of diapycnal mixing in the deep Indian Ocean apparent in Fig. 1 becomes more subtle as one moves northward, and could conceivably be in error because of a sampling bias in the distribution of CTD/LADCP transects. However, two factors give us confidence that the apparent zonal asymmetry is robust. First, there is a qualitative correspondence in the figure between turbulent mixing intensity and the presence of ridge-type topography, which is not surprising given the key role that this topography plays in various mechanisms of turbulent mixing in the abyssal ocean, be it powered by either tides or winds (e.g., Polzin et al. 1997; Thurnherr 2006; see also the discussion in Wunsch and Ferrari 2004). Ridge-type topography is far more widespread west of the Central Indian Ridge than east of it, suggesting that the apparent western intensification of diapycnal mixing in Fig. 1 is genuine. Second, as noted above, there is a qualitative correspondence between the in situ turbulent buoyancy flux estimates in the figure and the tidal energy dissipation estimates of Egbert and Ray (2001), which do not suffer from undersampling, and indeed show a western intensification of the rate of energy loss from the barotropic tide.

Because turbulent mixing drives the diapycnal water mass conversion underpinning the deep overturning of the Indian Ocean, and deep and bottom waters are observed to enter the region from the Southern Ocean over a wide zonal swath, with no obvious zonal bias (Ganachaud et al. 2000; Sloyan and Rintoul 2001), this suggests then that the Indian Ocean MOC may implicate substantial zonal exchanges between the various basins and even give rise to a significant zonal overturning circulation (ZOC). The existence of a zonal asymmetry in the intensity of diapycnal mixing and upwelling in the deep Indian Ocean is also hinted at by the potential vorticity (McCarthy and Talley 1999) and radiocarbon (Srinivasan et al. 2000) distributions at depth.

In this study, we will use a global eddy-permitting OGCM [the Ocean Circulation and Climate Advanced Modeling project (OCCAM); Webb et al. 1997] to investigate the existence and implications of a zonal dimension to the deep Indian Ocean MOC. Although the representation of diapycnal mixing in OCCAM is akin to parameterizations in other OGCMs that have proven to be unable to sustain a substantial deep overturning, the short OCCAM spinup allows the modeled density field to remain close to the climatological density distribution with which the model is initialized. The main effect of the short OCCAM run is to effectively interpolate the smooth climatological fields onto a finer grid in a dynamically consistent manner, introducing realistic boundary currents and fronts (Saunders et al. 1999). As a result, and by virtue of the geostrophic constraint,
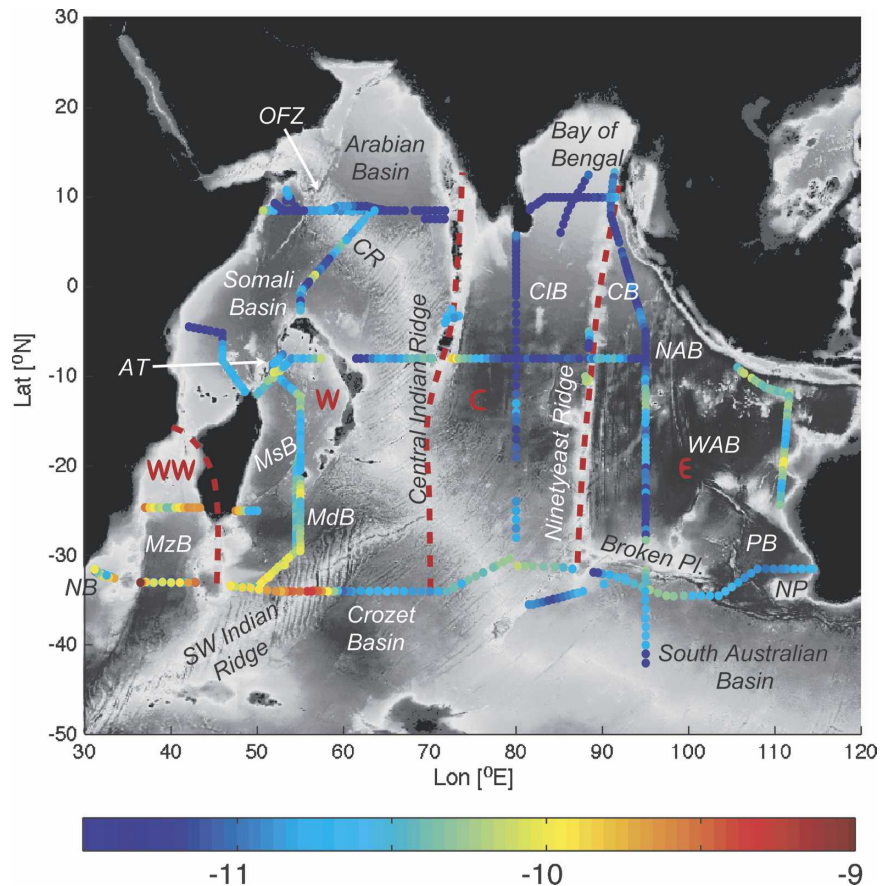
FIG. 1. Map of in situ estimates of the turbulent buoyancy flux $[(R_f/1 - R_f)\epsilon$, where $R_f = 0.15$ is the assumed flux Richardson number of the turbulence and ϵ is the rate of turbulent kinetic energy dissipation] associated with internal wave breaking at 3000 m in the Indian Ocean. The estimates are obtained by the application of an internal wave–wave interaction model to CTD/LADCP observations of density and velocity fine structure [see Kunze et al. (2006) for a detailed description of the estimation technique]. The topographic features of the Indian Ocean mentioned in the text are labeled (AT = Amirante Trench; CB = Cocos Basin; CIB = Central Indian Basin; CR = Carlsberg Ridge; MdB = Madagascar Basin; MsB = Mascarene Basin; MzB = Mozambique Basin; NAB = North Australian Basin; NB = Natal Basin; NP = Naturaliste Plateau; OFZ = Owen Fracture Zone; PB = Perth Basin; WAB = West Australian Basin). The most outstanding aspect of the distribution of the middepth turbulent buoyancy flux is its zonal asymmetry, with fluxes in the western basins of the Indian Ocean generally exceeding those in the central and eastern basins by an order of magnitude. The asymmetry is apparently related to the greater topographic complexity of the western basins and suggests that the breaking of internal tides may be a primary driver of the Indian Ocean MOC closure.

the circulation is primarily determined by the climatological density field and the topography. The model is described and its realism assessed in section 2. In section 3, we outline the Lagrangian methodology at the core of our analysis. The three-dimensional structure of the deep Indian Ocean overturning and its implications are discussed in section 4. Our analysis reveals that the deep Indian Ocean MOC is indeed associated with a considerable, depth-reversing zonal circulation, which constitutes ~½ of the MOC and has a major impact on

the residence time of tracers within the region. Section 5 provides a summary of our findings and some concluding remarks.

2. Model

a. OCCAM

The version of the OCCAM used in this study employs an Arakawa B grid, has 36 levels in the vertical and a uniform horizontal resolution of ¼° × ¼°. The

model has a free surface and uses Laplacian horizontal friction and diffusion. The horizontal diffusion coefficient for tracers is $100 \text{ m}^2 \text{ s}^{-1}$ and the horizontal viscosity coefficient is $200 \text{ m}^2 \text{ s}^{-1}$. A Richardson number–dependent scheme is implemented to represent the vertical mixing of tracers, with a background vertical diffusivity of $0.5 \times 10^{-4} \text{ m}^2 \text{ s}^{-1}$ prescribed in the deep ocean. In the deep ocean only the background diffusivity is operative. The vertical mixing coefficient for velocity is $10^{-4} \text{ m}^2 \text{ s}^{-1}$. The model bathymetry uses a cutoff of 5500-m depth and has discrete topographic steps associated with the depth of scalar grid boxes in the model. The model's bathymetry is slightly smoother than the outcome of a straight interpolation of the Shuttle Radar Topography Mission (SRTM) dataset (Becker and Sandwell 2004), but no marked differences are apparent.

For the purpose of this investigation, we use data from model years 9–11 of the OCCAM integration. The wind forcing is defined from 6-hourly European Centre for Medium Range Weather Forecasts (ECMWF) winds (Gibson et al. 1997), with years 9–11 of the model using wind stress fields from 1993 to 1995. Surface buoyancy fluxes are derived by relaxing the sea surface temperature and salinity to the *World Ocean Atlas 1994* (*WOA94*) climatology (Levitus and Boyer 1994; Levitus et al. 1994). The model's temperature and salinity fields are initialized with this same climatology.

Each model year produces 73 five-day averages for all model variables. Thus, the model climatology used throughout this investigation is constructed from the 219 archived five-day averages encompassed by model years 9, 10, and 11. The averaging of the velocity fields has been conducted in density space to account for the eddy-induced contribution (see Drijfhout et al. 2003). The *WOA94* product that was used for initialization clearly misses baroclinic gradients characterizing deep abyssal currents. However, this is (partly) remedied by the fact that after 9 yr of spinup, the model has been able to dynamically interpolate the large-scale density gradients of the *WOA94* product onto the high-resolution model grid. At this stage the flow has adjusted to the high-resolution model topography without changing the large-scale integrated density field substantially. Thus, large scales have been preserved, and small scales associated with boundary currents and deep inflows have been added during the 9-yr model spinup.

b. Model realism

The deep circulation of the Indian Ocean is shaped by the complex topographic configuration of the region, characterized by the presence of numerous ridges and basins (Fig. 2a). In the far west, deep waters from the South Atlantic and abyssal waters from the Weddell–Enderby Basin flow into the topographic enclosures of the Natal and Mozambique Basins and recirculate there (Toole and Warren 1993). A more significant pathway in the ventilation of the deep Indian Ocean conveys deep waters from the Antarctic Circumpolar Current and abyssal waters from the Weddell–Enderby Basin into the Crozet Basin (e.g., Toole and Warren 1993). As suggested by Fig. 2a, these waters experience a western-intensified northward flow into the Madagascar Basin through passages in the Southwest Indian Ridge, then flow into the Mascarene Basin (e.g., Warren 1981) and through the Amirante Trench into the Somali Basin (Johnson et al. 1991, 1998), and ultimately enter the Arabian Basin through the Owen Fracture Zone (Quadfasel et al. 1997). Diapycnal mixing along this path between the Madagascar and Arabian Basins causes the potential density of the deepest waters to decrease by up to $\sim 0.15 \text{ kg m}^{-3}$ (Mantyla and Reid 1995). In turn, the primary deep circulation pathway in the eastern Indian Ocean reflects the inflow of deep waters from the circumpolar region and abyssal waters from the Australian–Antarctic Basins into the South Australian Basin, from where these waters spread into the Perth Basin by flowing through the broad gap between the Broken and Naturaliste Plateaus (Toole and Warren 1993; Sloyan 2006; see Fig. 2a). After flowing north–northwestward into the West and North Australian Basins (e.g., Warren 1981), the deep and abyssal waters then enter the Central Indian Basin by overflowing the Ninetyeast Ridge at a number of sites, most notably at a passage near 11°S (Warren and Johnson 2002). We refer to Mantyla and Reid (1995) and Reid (2003) for more comprehensive reviews of the deep circulation of the Indian Ocean.

To convince the reader that, by virtue of its short spinup, OCCAM features a realistic deep Indian Ocean circulation in spite of its inaccurate parameterization of diapycnal mixing, we present a series of figures that enable comparisons with observational estimates of the circulation to be drawn. Figure 2b shows the average volume transport below 3500 m, an approximate upper bound for the inflow of deep waters in the model. Simultaneous inspection of Fig. 2a reveals that many of the important features of the deep flow field, as discussed above, are represented by the model: the entry and recirculation of deep water in the Natal and Mozambique Basins, the western-intensified northward pathway from the Crozet Basin to the Somali Basin, the north–northwestward spreading of deep water from the Perth Basin into the West and North Australian Basins, the subsequent flow over the Ninetyeast Ridge into the Central Indian Basin, and the lack of substantial deep
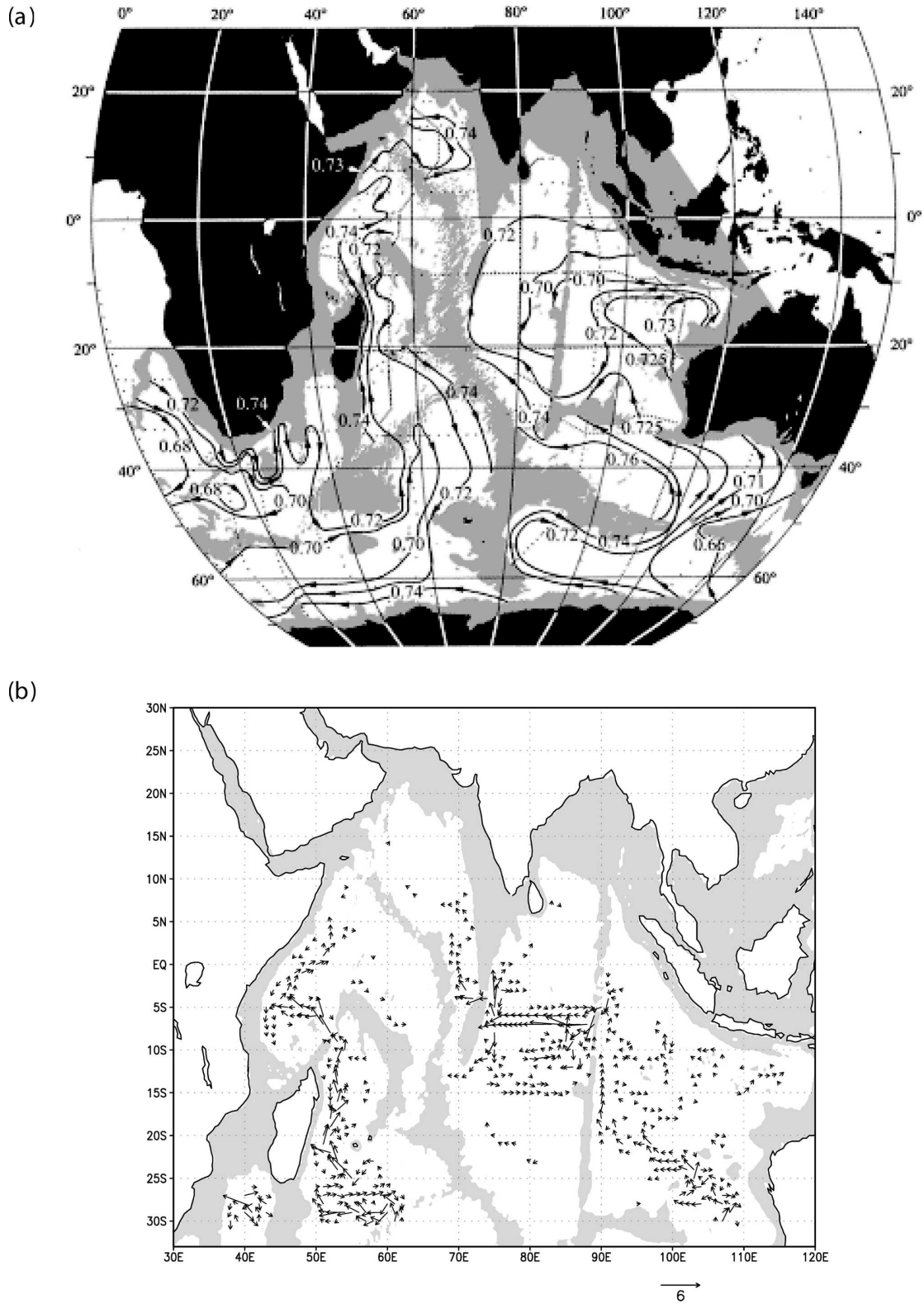
FIG. 2. (a) Adjusted steric height at 3500 db ($10 \ m^2 \ s^{-2}$), a proxy for the horizontal circulation in the lower limb of the deep Indian Ocean MOC. Depths less than 3500 m are shaded. (Reproduced from Reid 2003). (b) Map of the volume transport below 3500 m in OCCAM, gridded in $1° \times 1°$ bins and displayed as vectors with a cutoff value of 0.5 Sv. The vector scale is shown in the lower-right-hand corner of the figure. Depths less than 3500 m are shaded.

flow over the Central Indian Ridge. Minor qualitative differences are the apparently too-sluggish deep flows into the Somali and Arabian Basins in OCCAM; the location of the strongest zonal flow over the Ninetyeast Ridge near 5°S in the model, which is several degrees farther north than that observed; and the possibly overestimated deep flow from the Central Indian Basin to the Arabian Basin in OCCAM.

The deep circulation in OCCAM is primarily determined (through geostrophy and continuity) by the prescribed bottom topography and the large-scale density field with which the model is initialized. If OCCAM's representation of the Indian Ocean topography at ¼° × ¼° resolution is adequate, then the realism of the model's deep circulation implies that its deep density field has not departed significantly from the observed initial state. This point is illustrated in Fig. 3, where we compare the neutral density at the bottom of the Indian Ocean as featured in the state-of-the-art HydroBase climatology (Kobayashi and Suga 2006) with the neutral density at the deepest level in each grid point in OCCAM, which is initialized with the *WOA94* climatology. The Indian Ocean density field in OCCAM's years 9–12 is still rather realistic, because it preserves all major gradients on subbasin length scales greater than O(1000 km). However, there are numerous finescale differences introduced by the disparate resolutions of the (much smoother) *WOA94* climatology and the HydroBase climatology. The only appreciable larger-scale discrepancy is a slight bias toward excessively cold and fresh abyssal water masses in OCCAM, with these biases compensating almost exactly in neutral density.

The definitive test of the model's realism is provided by Fig. 4, which shows the deep Indian Ocean meridional overturning streamfunction in OCCAM as a function of neutral density and latitude. The MOC strength of nearly 6 Sv is somewhat weak in the context of estimates from observational studies, but it is rather vigorous in relation to the vast majority of OGCM-based estimates. The deep Indian Ocean MOC will likely weaken with time as the OCCAM run proceeds (Palmer et al. 2007), but for the period that we have chosen to analyze, the deep circulation remains moderately realistic. As for the MOC's vertical structure, the peak in the streamfunction occurs at $\gamma^n = 28.14$ kg m^{-3} or ~3500-m depth, near the boundary between the upper bottom water and the lower deep water. The occurrence of the bulk of the deep Indian Ocean inflow in these density classes is a recurrent feature in observational studies (e.g., Robbins and Toole 1997; Ganachaud et al. 2000), many of which exhibit a middepth outflow that is distributed over a somewhat wider vertical range than that in OCCAM. Nonetheless, all in all,

the deep Indian Ocean circulation in OCCAM does not display any obviously unrealistic features, and we will rely on this broad realism to justify our subsequent analysis. The basis for this justification is that a quantitative diagnosis of the deep Indian Ocean circulation for its own sake is beyond the scope of the present study. Rather, our aim is to convince the reader that the modeled flow field is realistic enough to permit its use in an investigation of the existence of a depth-reversing zonal circulation associated with the deep Indian Ocean MOC, which is suggested by the zonal asymmetry in the observational estimates of the turbulent buoyancy flux (Fig. 1).

3. Lagrangian methodology

Our investigation of the zonal dimension of the deep Indian Ocean MOC will rely on the use of a Lagrangian particle-tracking technique to quantitatively describe the overturning circulation in OCCAM. Our primary motivation for using this technique is that it allows us to single out water parcels involved in the overturning across neutral surfaces from those contributing to the large lateral recirculation of water entering and leaving the Indian Ocean with approximately the same density. A further advantage of this Lagrangian framework is that the dianeutral velocity of water parcels naturally follows from the divergence of the along-isopycnal mass transport, which is almost completely decoupled from the inaccurate vertical mixing parameterization of the model during the short spinup run analyzed here.

a. Particle-tracking algorithm

The tracing technique used in this study was originally developed by Döös (1995) and Blanke and Raynaud (1997). It calculates the three-dimensional path of water particles offline from the model data. An efficient implementation of the algorithm allows for the calculation of thousands to millions of trajectories for very long periods. As a result, the importance of the different routes followed by individual water masses can be quantified. First, sections are defined where the trajectories start and stop. The number of trajectories that start at the sidewall of a grid box is taken to be proportional to the transport through that sidewall, where the transport may be confined to a certain density or depth interval. Within each grid box, the particles are equally distributed over the sidewall that coincides with the starting section. Because the particle seeding in each grid box is proportional to the transport across the sidewall where the particles start, each particle can be associated with a fixed transport, and each

(a)

Bottom neutral density in the Indian Ocean

(b)

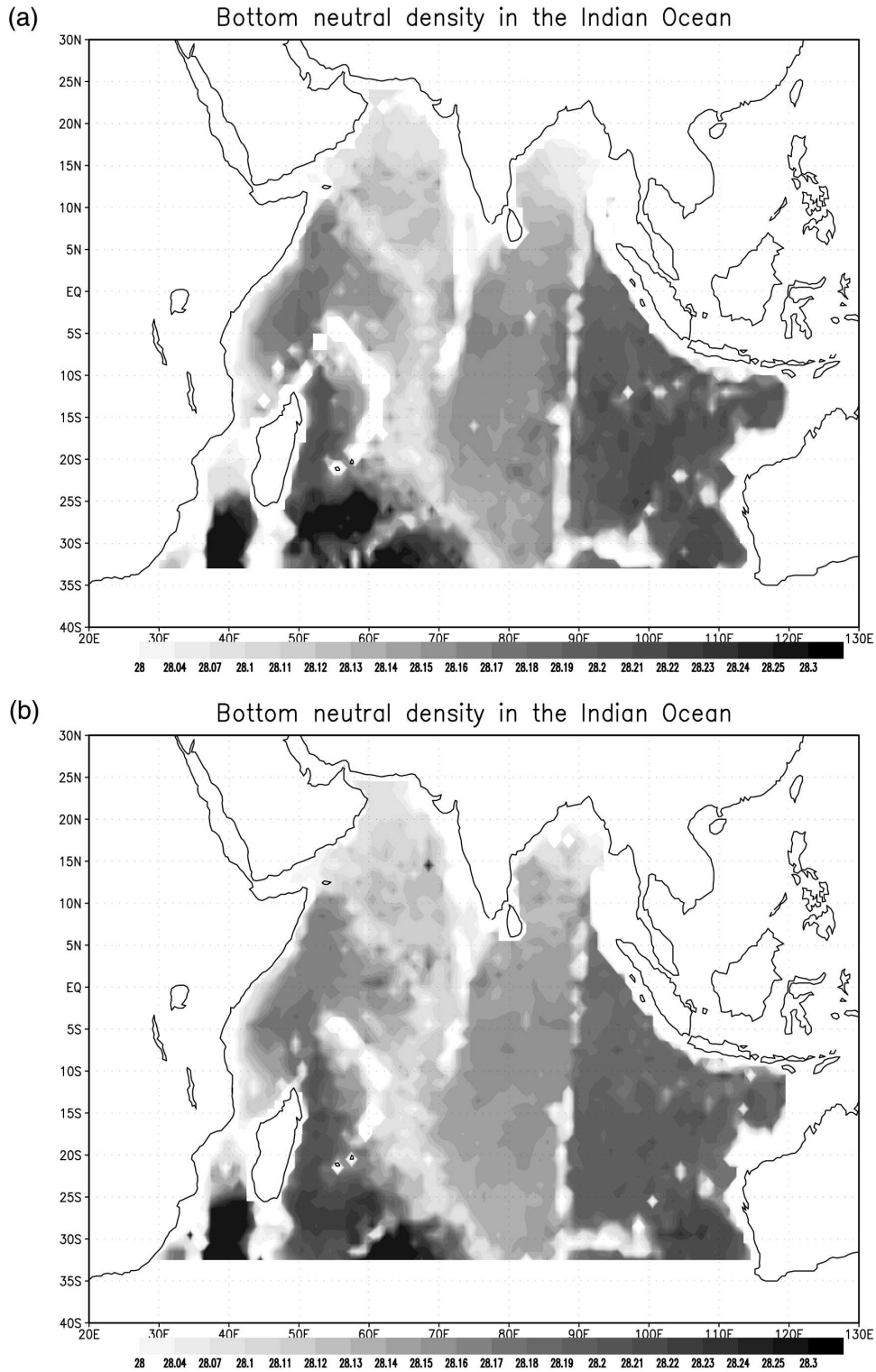## Bottom neutral density in the Indian Ocean

FIG. 3. Neutral density (a) at the bottom of the Indian Ocean from the HydroBase (Kobayashi and Suga 2006) and (b) at the deepest level in each OCCAM Indian Ocean grid point. Neutral densities lower than $\gamma^n = 28.0$ are masked.
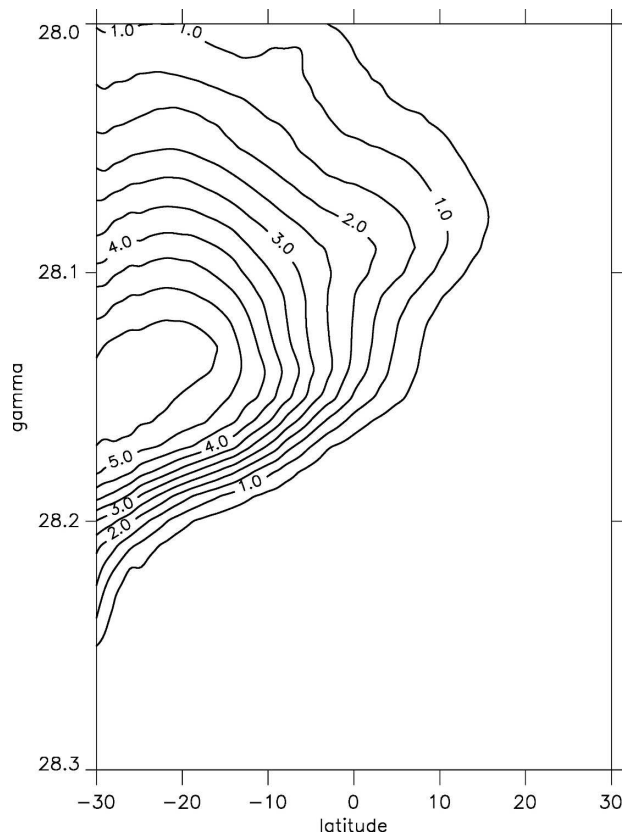
FIG. 4. Meridional overturning streamfunction in the deep Indian Ocean as a function of neutral density and latitude. The existence of the Indonesian Throughflow does not affect this overturning cell, because the inflow from the Pacific occurs at densities lighter than $\gamma^n = 28.0$ kg m^{-3}.

particle trajectory becomes a well-defined streamfunction. It follows that particle trajectories can be added together. With this method particles can be tracked forward, as well as backward, in time. The trajectory stops when one of the predefined end sections has been reached. It should be noted that this method calculates the advective path of particles.

The algorithm to calculate particle trajectories uses an exact analytical solution of the particle path within each grid box. This solution can be obtained when the velocity or transport across each of the six sidewalls of a grid box is given, assuming that within the grid box this velocity varies linearly between every pair of opposing sidewalls. We refer to Döös (1995) for the exact analytical solution. The algorithm calculates both the transit time for each grid box, and the sidewall and position where the particle leaves the grid box. This end position serves as the initial position for the neighboring grid box, and the calculation can be repeated until the sidewall where the particle exits the grid box coincides with one of the predefined end sections.

The velocity field used for this calculation includes an eddy-induced transport velocity calculated from the temporal correlation between velocity and isopycnal thickness variations. This calculation was conducted by transforming a 5-day-averaged OCCAM velocity field "snapshot" from z to density (σ_2) coordinates, computing the time-mean isopycnal mass transport, and transforming this quantity back to z coordinates. For further details on the calculation we refer to Drijfhout et al. (2003).

We employ a time-independent velocity field in our calculation of particle trajectories. Initially, we considered using a time-dependent algorithm to resolve the seasonal cycle in the Indian Ocean circulation, but were dissuaded by the occurrence of a strong seasonal signal of uncertain origin at depths in excess of 2000 m. We were unsure whether this signal was either associated with a realistic barotropic response to intense monsoonal shifts in the atmospheric forcing, or linked to an undersampling of high-frequency flows in the model. At any rate, we conducted a series of sensitivity tests that assured us of the negligible impact that ignoring the temporal variability of the flow has on our diagnostics of the deep Indian Ocean overturning.

b. Lagrangian upwelling

In OCCAM, the diapycnal velocity is largely determined by the inaccurate parameterization of diapycnal mixing. However, because the model has not reached a steady state, the divergence of the isopycnal mass transport does not exactly balance the diapycnal mass transport set by the diapycnal diffusivity, and so the model is subject to drift. In the following, we argue that the divergence of the isopycnal mass flux during the early model spinup is a far more accurate estimate of the true diapycnal mass transport than the flux associated with the model's explicit diapycnal diffusivity. Although the latter ultimately shapes the model's steady state, it is the former that drives the upwelling of water parcels across subsurface isopycnals. In the spinup phase, these two quantities are entirely different.

To illustrate this point, we consider the continuity equation in an isopycnic framework:

$$\frac{\partial h}{\partial t} = -\boldsymbol{\nabla} \cdot (\mathbf{u}h) + \Delta w_{\mathrm{dia}}, \tag{1}$$

where $\mathbf{u}$ is the two-dimensional isopycnal velocity, h is the thickness of a layer bounded by two isopycnal surfaces, and

$$\Delta w_{\mathrm{dia}} = w_{\mathrm{dia}(+)} - w_{\mathrm{dia}(-)}, \tag{2}$$

where the $+/-$ refer to the upper and lower bounding isopycnals of the layer, respectively, and w_{dia} is the diapycnal velocity given by

$$w_{dia} = \frac{\partial}{\partial z}\left(K\frac{\partial \rho}{\partial z}\right)\bigg/\frac{\partial \rho}{\partial z}. \tag{3}$$

Assuming that the true system is close to a steady state or that our observations span a long enough period to justify this assumption, we can write (1) as

$$0 = -\nabla \cdot (\mathbf{u}h)_{true} + \Delta w_{dia\text{-}true}, \tag{4}$$

where the subscript "true" refers to quantities characterizing the real ocean flow. The equivalent expression for OCCAM, which starts drifting immediately after initialization, primarily as a result of the inaccurate parameterization of diapycnal diffusivity in the model (Lee et al. 2002), is

$$0 = -\nabla \cdot (\mathbf{u}h)_{mod} + \Delta w_{dia\text{-}mod} + \Delta w_{drift}, \tag{5}$$

where the subscript "mod" refers to quantities characterizing the modeled ocean flow, and we define

$$\Delta w_{drift} = -\frac{\partial h}{\partial t}. \tag{6}$$

If the modeled density field remains close to the initial state and, through geostrophy, the circulation is broadly realistic, then

$$\nabla \cdot (\mathbf{u}h)_{mod} \simeq \nabla \cdot (\mathbf{u}h)_{true}. \tag{7}$$

Using (4), (5), and (7), it follows that

$$\Delta w_{dia\text{-}true} = \Delta w_{dia\text{-}mod} + \Delta w_{drift}. \tag{8}$$

Thus, we argue that despite the inadequate parameterization of diapycnal diffusivity in the model, Lagrangian particles should feel an effective diapycnal velocity that is close to the true one as long as the isopycnal mass flux divergence field has not drifted too far away from its initial state. We stress that this statement will only hold for a set of time-mean density and velocity fields in which unrealistic wave motions associated with the model's dynamical adjustment to either the initial state or model drift have been sufficiently well sampled and averaged out. Given a relatively short model spin-up time of 9 yr and our choice to analyze 3-yr mean density and velocity fields, we believe that our evaluation of OCCAM satisfies the above conditions. This belief is endorsed by our assessment of the model's realism in section 2b.

In the present study, we work with only one bounding isopycnal and integrate from the bottom to that isopycnal. Thus, h is always the thickness of the column of water denser than a certain neutral density value. In that case, Eq. (8) becomes

$$w_{dia\text{-}true} = w_{dia\text{-}mod} + w_{drift}. \tag{9}$$

Note that the w_{dia} we diagnose from the particle-tracking method is not exactly equal to the divergence of the mass flux in the model $w_{dia\text{-}mod}$, which contains the eddy flux as well (unlike the Eulerian mean w that is carried by the model). Here, $w_{dia\text{-}mod}$ features much small-scale variability, with double-signed patterns on the eddy scale. As a result, a water parcel is often subject to a series of up- and downwelling events that are separated by small horizontal distances and characterized by small vertical extents in both depth and density coordinates. With the particle-tracking method we choose one such crossing event (the first crossing), which effectively removes the unwanted small-scale noise in the upwelling/downwelling pattern of the model.

4. A Lagrangian view of the deep Indian Ocean overturning

To describe the three-dimensional structure of the deep Indian Ocean overturning and investigate its implications, we trace the particles entering the Indian Ocean across its southern boundary within the lower limb of the overturning forward in time. Our selection criterion is that particles must cross a section extending between Africa and Australia along 30°S in a northward direction and with density in excess of $\gamma^n = 28.14$ kg m^{-3}, the neutral surface at which the meridional overturning streamfunction peaks (Fig. 4). Particles are seeded in proportion to the northward transport in each model grid cell, where each particle is associated with a volume transport of about 250 m^3 s^{-1}. A particle's trajectory ceases to be traced when the particle leaves the Indian Ocean through its eastern boundary with the Indonesian seas (a minor fraction of all particles) or when it crosses the section at 30°S in a southward direction. Within the latter group of particles, those outflowing the Indian Ocean with a density higher than $\gamma^n = 28.14$ kg m^{-3} are considered to be part of a recirculating gyre component of the deep Indian Ocean circulation (or possibly a weak reversed overturning circulation, which in the zonal mean is disguised by the dominant overturning cell), whereas lighter particles are regarded as contributing to the deep overturning circulation. Using this distinction, we effectively isolate the water parcels participating in the deep Indian Ocean overturning and, in the following, are able to identify their circulation pathways and upwelling sites.

a. The deep circulation

Figure 5a shows the initial and final positions of the particles participating in the deep Indian Ocean over-

(a)

Positions at 30S of the deep overturning cell

(b)
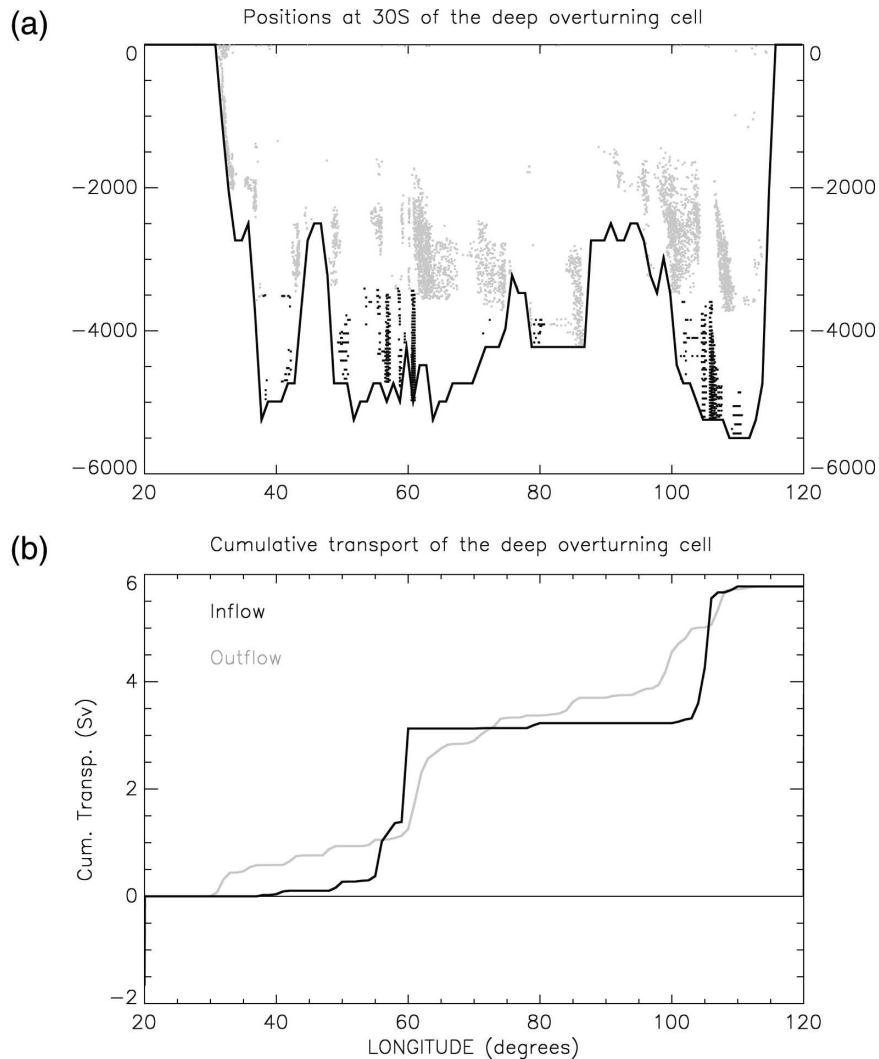
Cumulative transport of the deep overturning cell

FIG. 5. (a) Cross-sectional view of the deep Indian Ocean overturning circulation at 30°S. Black dots denote northward-flowing particles, with gray dots representing southward-flowing particles. A transport of about 250 m^3 s^{-1} is associated with each particle. The thick black line denotes the bottom topography at 30°S. (b) Cumulative transport of the inflow (black) and outflow (gray) across 30°S associated with the deep Indian Ocean overturning circulation. Transports are integrated from west to east.

turning circulation in OCCAM, at the 30°S section. Both inflow and outflow positions display considerable banded structure, indicating that the deep overturning is effected by narrow currents with a vertical extent of 1000–2000 m and a width that is often of the order of 100 km. The bandedness is particularly pronounced for the inflow positions.

The bulk of the inflow occurs between 3500- and 5000-m depth and is concentrated in two sites (Fig. 5b). Approximately 3 Sv of water flow northward in the eastern Madagascar Basin in the 55°–60°E zonal band, whereas 2.5 Sv do so along the eastern flank of the West Australian Basin near 110°E. The transport involved in

the western route is in broad agreement with both the 2.5–3.8-Sv northward transport of bottom water in the Mascarene Basin that was estimated by Johnson et al. (1998) using a thermal wind calculation and its gradual decay to values of 1.0–1.7 Sv in the Amirante Passage (Fieux and Swallow 1988; Johnson et al. 1998) and 1.2–2.3 Sv in the Owen Fracture Zone (Johnson et al. 1991; Quadfasel et al. 1997; Dengler et al. 2002). The broad realism of the transport implicated in the eastern route may be slightly diminished, because observations suggest that approximately 4 Sv enter the Perth Basin below 3500 m (Sloyan 2006). Minor inflows of the order of 0.1 Sv are detected in the Mozambique Basin and near

80°E, where a deep passage in the Central Indian Ridge permits flow into the Central Indian Basin. In turn, much of the outflow occurs between 2000 and 3500 m depth. Only 0.5 Sv of the upwelled deep and bottom waters are transformed into intermediate and thermocline waters, leaving the Indian Ocean in the Agulhas Current and upwelling into lighter classes outside the Indian Ocean. An overwhelming fraction of the Agulhas Current is instead derived from water entering the Indian Ocean in intermediate and thermocline densities, in clear disagreement with "conveyor belt"–like descriptions of the global ocean circulation (e.g., Broecker 1991). We note that the outflowing limb of the Indian Ocean MOC is more evenly distributed with longitude than the inflow, and forms relatively broad currents above the Central Indian Ridge and in the West Australian Basin.

An overview of the circulation pathways involved in the deep Indian Ocean overturning is provided by Fig. 6, which shows Lagrangian transport vector maps for the inflow (Fig. 6a) and outflow (Fig. 6b) limbs of the overturning. The transport vectors are calculated by integrating the mass transport carried by particles across each side of a certain grid box. The gridbox size for this calculation does not need to coincide with the OCCAM gridcell size. Here we use $1° \times 1°$ grid boxes. The transport vectors of the deep inflow suggest a very similar picture to that of the Eulerian transport below 3500-m depth (Fig. 2b). In the western Indian Ocean, the dominant pathway is directed into the Madagascar Basin, initially along its eastern flank and then along its western flank north of 25°S. The pathway is prolonged northward into the Mascarene Basin, where the deep inflow turns northwestward and overflows the Amirante Trench into the Somali Basin. North of this basin, it is largely halted by the Carlsberg Ridge, which prevents significant flow into the Arabian Basin. Additional northward transport into the western Indian Ocean is seen to occur in the Mozambique Basin, but because this represents a topographic enclosure to bottom water inflow, the transport is only weak.

The primary pathway of deep flow into the eastern Indian Ocean is directed northwestward from the Perth Basin. Near 20°S, the pathway meets the eastern flank of the Ninetyeast Ridge and subsequently veers northward. A secondary pathway follows the eastern flank of the West Australian Basin from 30°S and turns westward near 10°S to join the primary pathway at the Ninetyeast Ridge. While a weak branch of the inflow continues northward along the eastern flank of the ridge, the main flow over the ridge takes place through a passage near 5°S. This gap has been shown to host substantial westward bottom flow in the real ocean (War-

ren and Johnson 2002), but lies to the north of the main overflow site at 11°S, as identified by Warren (1982). Inspection of the model bathymetry and comparison with a straight interpolation of high-resolution bathymetry on the 0.25° grid reveals no peculiarities indicating that the model bathymetry should be unrealistic, and the cause for the model's incorrect choice of primary overflow passage is unclear. Regardless, it is likely that this choice has little impact on the large-scale character of the pathway. After overflowing the ridge, the pathway turns southward initially, and then resumes its westward flow across the Central Indian Basin as a near-zonal current near 6°S. The pathway splits into a northward and a southward branch in encountering the eastern flank of the Central Indian Ridge. These two branches (inferred from the Lagrangian streamfunction, not shown) go on to ventilate the northern and southern regions of the deep Central Indian Basin. Generally speaking, all of the deep inflow pathways outlined above compare favorably with observational estimates of the deep circulation (e.g., Mantyla and Reid 1995; McCarthy and Talley 1999; Reid 2003).

The circulation of the outflowing upper limb of the overturning is more complex. Nonetheless, it is obvious that its strongest flows are often biased westward with respect to those implicated in the inflowing lower limb of the overturning. The velocity field of the Central Indian Basin is especially convoluted and exhibits a strong recirculating component that is hinted at by the middepth steric height maps of Reid (2003) and the pattern of spreading of terrigenic helium plumes in the central Indian Ocean reported by Srinivasan et al. (2004).

The outflowing deep water follows four main pathways out of the basin that also appear to be suggested by observations. One of these pathways follows the eastern flank of the Central Indian Ridge in a northward direction and is then steered northeastward into the Bay of Bengal, from where it returns southward in a more diffuse form that is imperceptible in Fig. 6b. The other three routes have in common their involvement of a southward current following the African margin as far south as 5°–10°S. This current is fed from three different locations: directly from the northwestern edge of the Somali Basin, where some of the inflowing bottom water upwells; from the Central Indian Basin, by overflowing the Central Indian Ridge near 10°S; and again, from the Central Indian Basin, by entering the Arabian Basin after negotiating the intersection between the Carlsberg and Central Indian ridges. Before leaving the Indian Ocean, the southward current along the African margin splits into three branches: a small fraction of particles crosses the Mozambique Channel
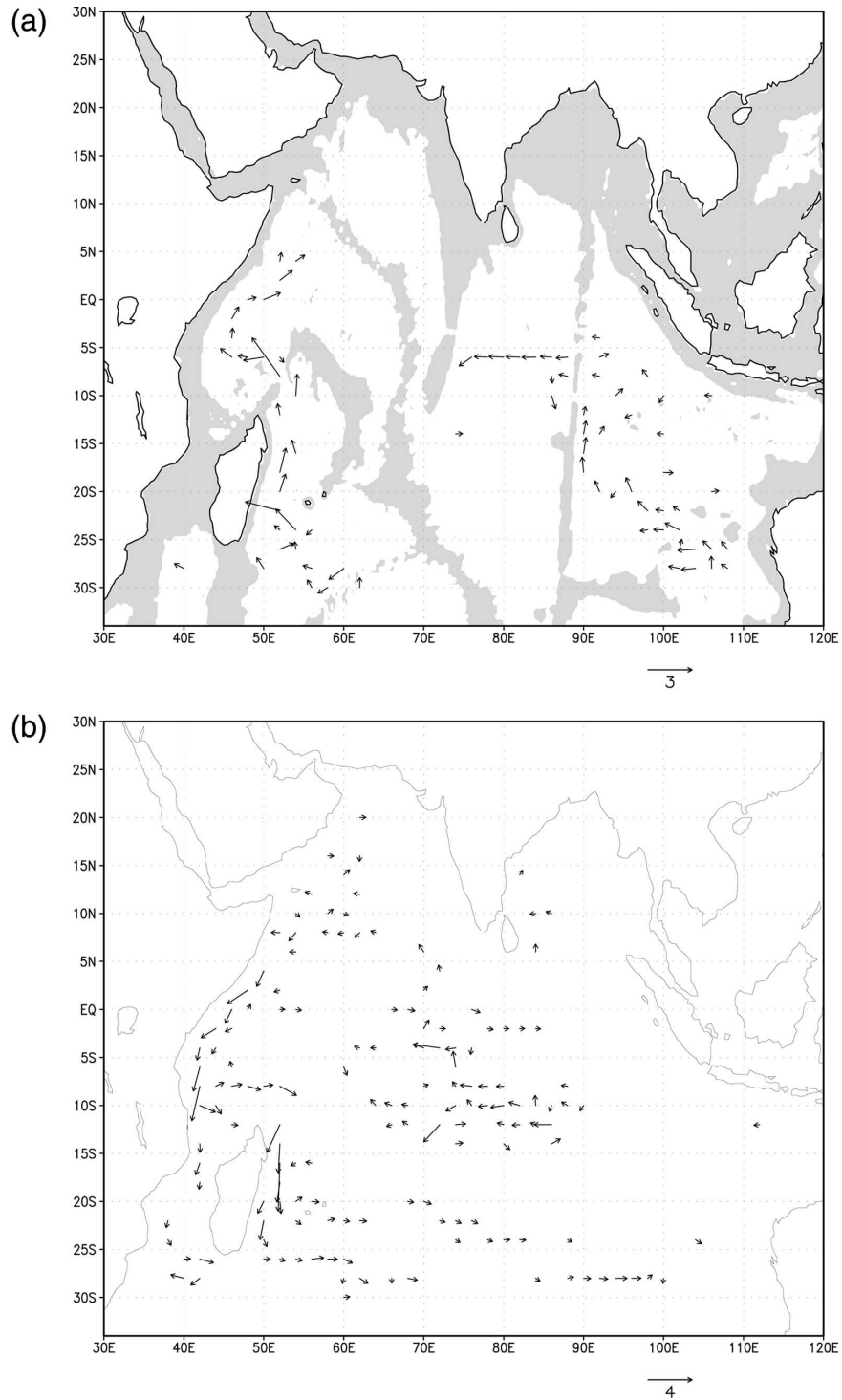
FIG. 6. (a) Map of Lagrangian transport vectors associated with the deep inflow for particles with $\gamma^n > 28.14$ kg m^{-3}. The vectors are calculated by integrating the zonal and meridional mass transports in $1° \times 1°$ grid boxes, and are plotted every second grid point with a cutoff value of 0.2 Sv. The scaling is indicated below the lower axis of the figure. Regions deeper than 3500 m are shaded. (b) Same as (a), but for outflowing particles with $\gamma^n < 28.14$ kg m^{-3}.
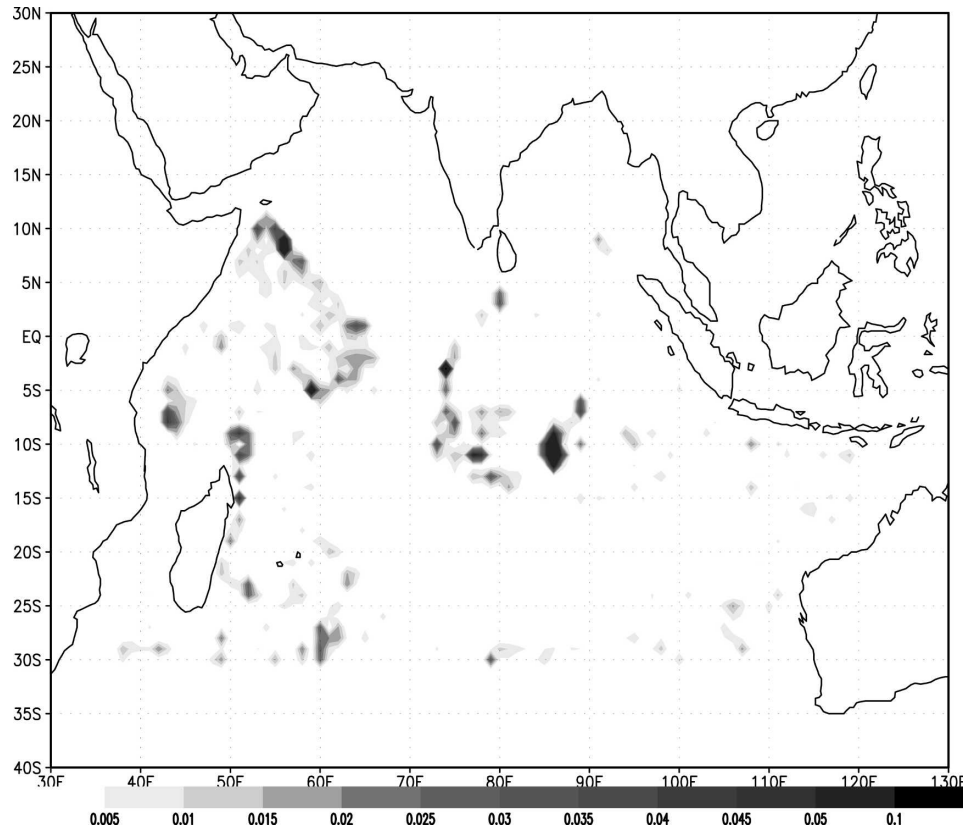
FIG. 7. Upward diapycnal volume transport across the $\gamma^n = 28.14$ kg m^{-3} surface. Units are Sverdrups per $1° \times 1°$ grid box. A zonal asymmetry in upwelling is apparent, with enhanced upwelling in the western part of the Indian Ocean.

and contributes to the Agulhas Current; a larger proportion is diverted southeastward into the Mascarene and Madagascar basins, from which it leaves the Indian Ocean; and a final branch follows the eastern flank of the Central Indian Ridge initially, and then proceeds eastward along the northern edge of the Broken Plateau before escaping on both sides of the West Australian Basin. In agreement with this latter pathway, eastward return flow through the sills in the Ninetyeast Ridge near 28°S was observed by Warren and Johnson (2002).

The inflowing and outflowing limbs of the deep Indian Ocean overturning are connected by a diapycnal mass transport across the $\gamma^n = 28.14$ kg m^{-3} surface. Figure 7 shows the geographical distribution of this transport. Some of the diapycnal upwelling sites had already been suggested by Fig. 6a as the ridges where the deep inflow appears to halt, for example, the Carlsberg Ridge (for the primary pathway into the western Indian Ocean), and the Central Indian Ridge (for that into the eastern Indian Ocean). Additionally, the model shows enhanced upwelling around Madagascar, with "hot spots" near the sill of the Amirante Trench north-

east of the island (Barton and Hill 1989) and near 85°E, 10°S over the western flank of the Ninetyeast Ridge, at a site where a westward protrusion of the ridge blocks southward bottom flow. Less pronounced diapycnal-upwelling hot spots are found near 79°E, 30°S, downstream of the southernmost sill in the Ninetyeast Ridge (McCarthy et al. 1997), over the Southwest Indian Ridge, and near 8°S, 43°E, in an area where topography intercepts westward bottom flow off the African coast.

It would be naive to expect OCCAM to reproduce in detail the distribution of the turbulent buoyancy flux in Fig. 1. However, it is clear from Fig. 7 that the model retains the broad zonal asymmetry in the deep overturning circulation closure that is suggested by the observations. The OCCAM Indian Ocean flow field is thus in accord with our basic hypothesis that the upwelling closing the deep Indian Ocean overturning circulation occurs primarily in the western side of the ocean and, on average, westward of the sites where deep inflow occurs at the southern boundary. This appears to imply the existence of a depth-reversing zonal circulation in both the real and modeled Indian Ocean.

TABLE 1. Decomposition of the deep Indian Ocean MOC according to the location of inflow, upwelling, and outflow in one of four zones, namely, WW (far west), W (west), C (central), and E (east); see text for a description of how to associate these zones with particular Indian Ocean basins and Fig. 1 for a plan view map. Combinations involving less than 0.1 Sv have been omitted. Combinations involving the same zone for inflow, upwelling, and outflow may contribute to either the direct or the indirect overturning. The latter is the case if the inflow or outflow pathway transgresses the boundaries of the relevant zone. In this instance the partitioning between direct and indirect overturning is indicated by the suffixes (dir) and (ind), respectively. The two numerical columns indicate the volume transport and mean residence time in the Indian Ocean of each component. The last column indicates whether the component follows the mean sense of the depth-reversing zonal circulation (+), acts in the opposite sense (−), or makes no contribution to the zonal circulation (0).

WW/WW/WW (dir)	0.1 Sv	70 yr	0
W/W/W (dir)	1.5 Sv	80 yr	0
W/W/W (ind)	0.3 Sv	440 yr	0
W/W/WW	0.3 Sv	440 yr	0
W/W/C	0.1 Sv	310 yr	+
W/W/E	0.8 Sv	340 yr	+
C/C/C (dir)	0.1 Sv	10 yr	0
E/E/E (dir)	0.3 Sv	160 yr	0
E/E/E (ind)	0.2 Sv	630 yr	0
E/C/E	0.7 Sv	530 yr	+
E/E/WW	0.1 Sv	700 yr	−
E/C/WW	0.2 Sv	880 yr	+
E/E/W	0.2 Sv	550 yr	−
E/C/W	0.5 Sv	530 yr	+
E/C/C	0.2 Sv	460 yr	+

b. The depth-reversing zonal circulation

To explicitly demonstrate the existence of such a circulation, we decompose the deep Indian Ocean overturning into a number of different components defined on the basis of where inflow, upwelling, and outflow occur. In defining the location of any of these events, we distinguish four Indian Ocean zones (Fig. 1): zone WW (the far west) comprises the Mozambique Basin; zone W (west) encompasses the Madagascar, Mascarene, Somali, and Arabian Basins; zone C (central) refers to the Central Indian Basin and the Bay of Bengal; and zone E (east) spans the West Australian, North Australian, and Cocos Basins. Table 1 shows the results of a decomposition of the deep overturning in these terms.

The deep Indian Ocean MOC has an amplitude of 5.6 Sv. A partitioning into direct and indirect overturning circulation (with the direct overturning implying inflow, upwelling, recirculation, and outflow all confined to the same zone) yields a direct overturning of 2.0 Sv and an indirect overturning of 3.6 Sv. Thus, around 65% of the deep MOC is associated with exchange between different zones. But does this exchange between

different zones give rise to an apparent ZOC? (The ZOC streamfunction is a useful diagnostic of the depth-reversing zonal circulation, because this circulation must take the appearance of a zonal overturning when the Indian Ocean zonal transport is integrated in the meridional direction.) In answer to this question, we note that of the 3.6 Sv implicated in the indirect overturning, (i) 1.2 Sv flow into and out of the Indian Ocean in the same zone (when inflow and outflow in the same zone is accompanied by recirculations that extend over various zones, the overturning is considered to be indirect), (ii) 1.5 Sv leave the Indian Ocean west of their inflow zone, and (iii) 0.9 Sv flow out of the Indian Ocean east of their inflow zone. Case (i) contributes to an apparent ZOC if upwelling occurs west of the inflow and outflow; case (ii) contributes to an apparent ZOC if upwelling occurs in the outflow zone; and case (iii) contributes to an apparent ZOC if upwelling occurs in the inflow zone. To further illustrate the apparent ZOC, we refer to several meridional integrations (from 30°S to the northern boundary) of zonal transport at selected longitudes (Fig. 8). This figure indeed shows westward flow at dense levels and eastward flow in lighter classes.

Close inspection of the decomposition in Table 1 reveals that 2.5 Sv (or around 45%) of the deep Indian Ocean MOC in OCCAM contributes to an apparent ZOC characterized by predominantly westward flow at great depth and predominantly eastward flow at a shallower, middepth level. A mere 0.3 Sv flows in the opposite sense to this meridionally integrated, depth-reversing zonal circulation. The reason that these two contributions do not add up to 3.6 Sv (the size of the indirect overturning) is that 0.8 Sv flow into and out of the Indian Ocean in the same basin, but with excursions into other basins in between inflow and outflow.

We note that our zonal decomposition artificially excludes contributions to the depth-reversing zonal circulation from water parcels in the direct overturning that upwell to the west of their inflow and outflow sites, albeit within the same zone. Figure 7 suggests that this contribution may be significant, because many upwelling sites lie near the western boundary of the western and central Indian Ocean Basins. In synthesis, the decomposition in Table 1 is consistent with the existence of a depth-reversing zonal circulation that is approximately half as strong as the MOC.

The association between the various components of our decomposition and the deep Indian Ocean circulation pathways outlined in section 4a is illustrated by Fig. 9, which shows the initial and final positions at 30°S of particles participating in either the direct or indirect overturning. For the latter, we have discriminated be-
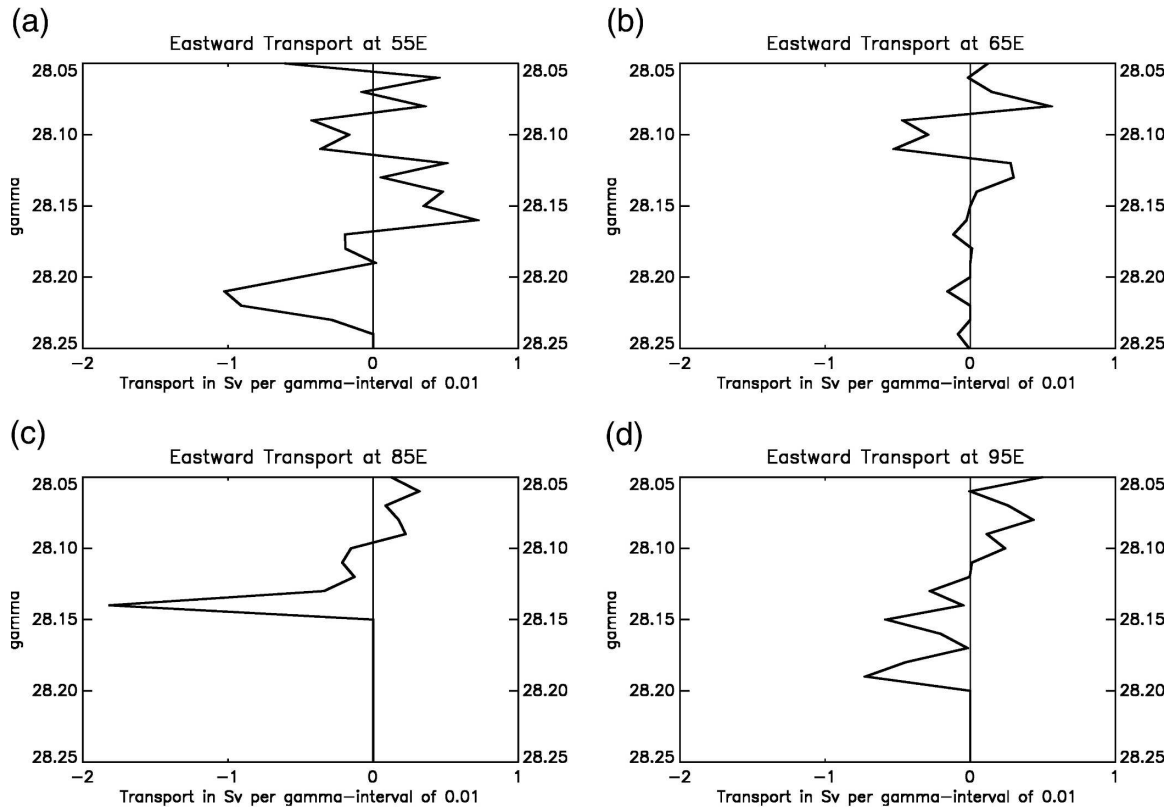
FIG. 8. Zonal transport as a function of gamma with binning in intervals of 0.01 at (a) 55°, (b) 65°, (c) 85°, and (d) 95°E.

tween particles inflowing to the Indian Ocean in zone W and those inflowing in zone E. Note that all of the particles inflowing in zones WW (the Mozambique Basin) and C (the Central Indian Basin) participate in the direct overturning circulation.

The direct overturning circulation (Fig. 9a) is dominated by inflow in the W zone (the Madagascar Basin). About 50% of the inflow in this zone participates in the direct overturning. The bulk of the outflow occurs slightly to the east of the main inflow sites. The indirect overturning circulation associated with the western inflow (Fig. 9b) is somewhat smaller (1.5 Sv) than the indirect cell associated with the eastern inflow (2.1 Sv; see Fig. 9c). The outflow sites are similar in both cases and appear to be distributed over all four zones.

The deep circulation pathways connecting inflow and outflow sites are, however, very different for the indirect overturning cells respectively associated with the western and eastern inflows. Figure 10 displays these pathways in terms of the Lagrangian streamfunction. The direct overturning features inflow into the Madagascar Basin that continues northward along the western Indian Ocean as far as the Arabian Basin. The outflow follows a similar pathway in the opposite direction, turning southeastward south of 25°S. The direct

overturning in the eastern Indian Ocean is weak and rather diffuse, as might be expected from the concentration of diapycnal mixing hot spots in the western and central Indian Ocean.

The indirect overturning associated with the western inflow exhibits similar pathways to the direct overturning. The only significant difference is the presence of a weak large-scale recirculation in the former, extending along the equatorial region with westward flow between 5° and 10°S and eastward flow near the equator. The northern branch of this recirculation is reminiscent of the observations of equatorial deep jets south of the Indian subcontinent (e.g., Luyten and Swallow 1976; Ponte and Luyten 1990; Dengler and Quadfasel 2002). Dengler and Quadfasel (2002) report bottom-reaching jets sharing several features with the equatorial deep flow in the OCCAM Indian Ocean, particularly their reversing direction both with depth and distance off the equator. Nonetheless, Dengler and Quadfasel propose that the jets may be the signatures of first meridional mode equatorial Rossby waves, in which case their persistence over periods longer than a year would be uncertain. We note also that the outflow branch of the indirect overturning displays an anticyclonic circulation in the Southern Hemisphere tropics and a weak anti-
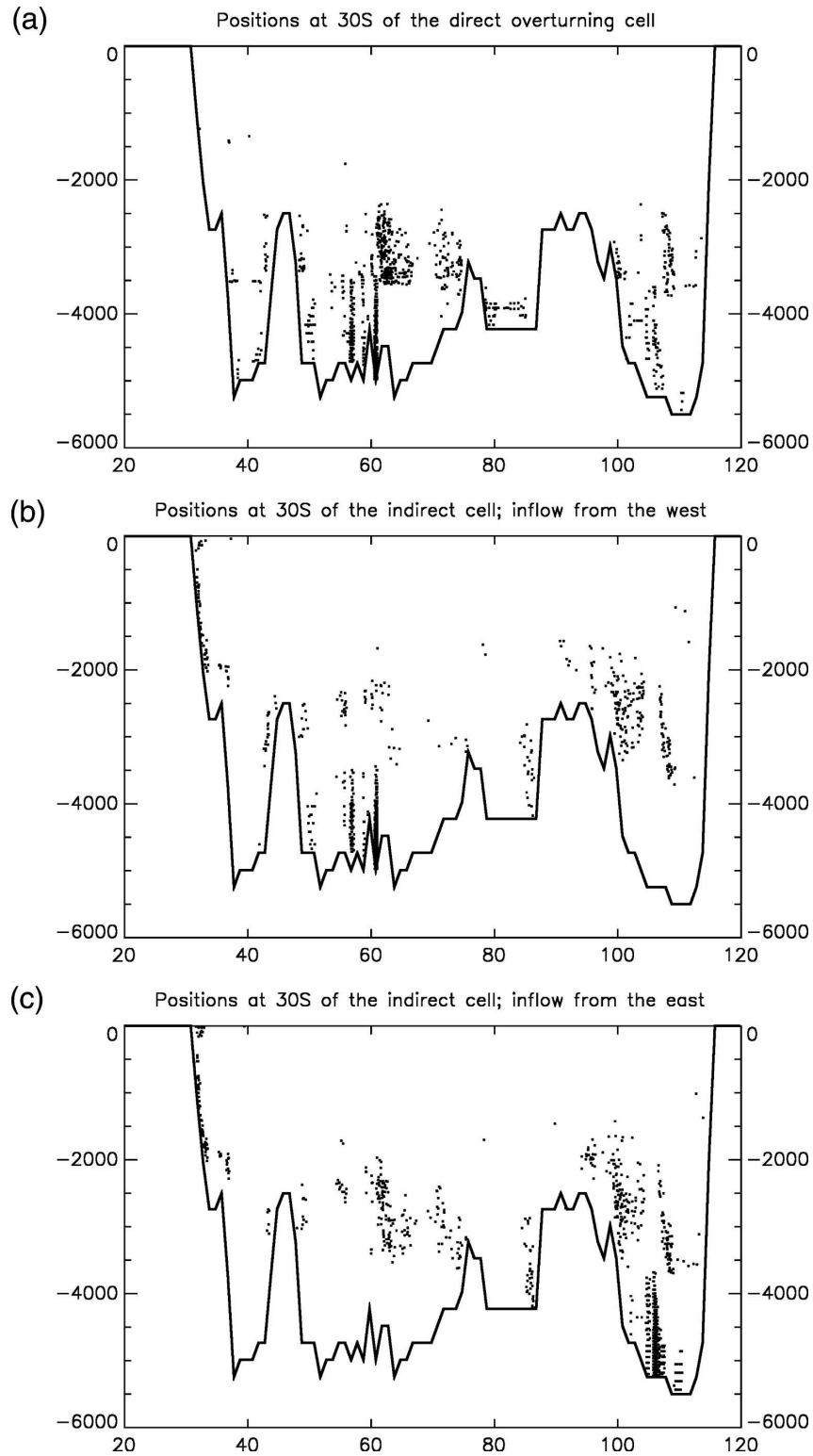
FIG. 9. (a) Cross-sectional view of (a) the direct overturning circulation in the Indian Ocean at 30°S, and (b), (c) the indirect overturning associated with the western and eastern inflows. Black (gray) dots denote northward (southward) flowing particles. The thick black line denotes the bottom topography at 30°S.
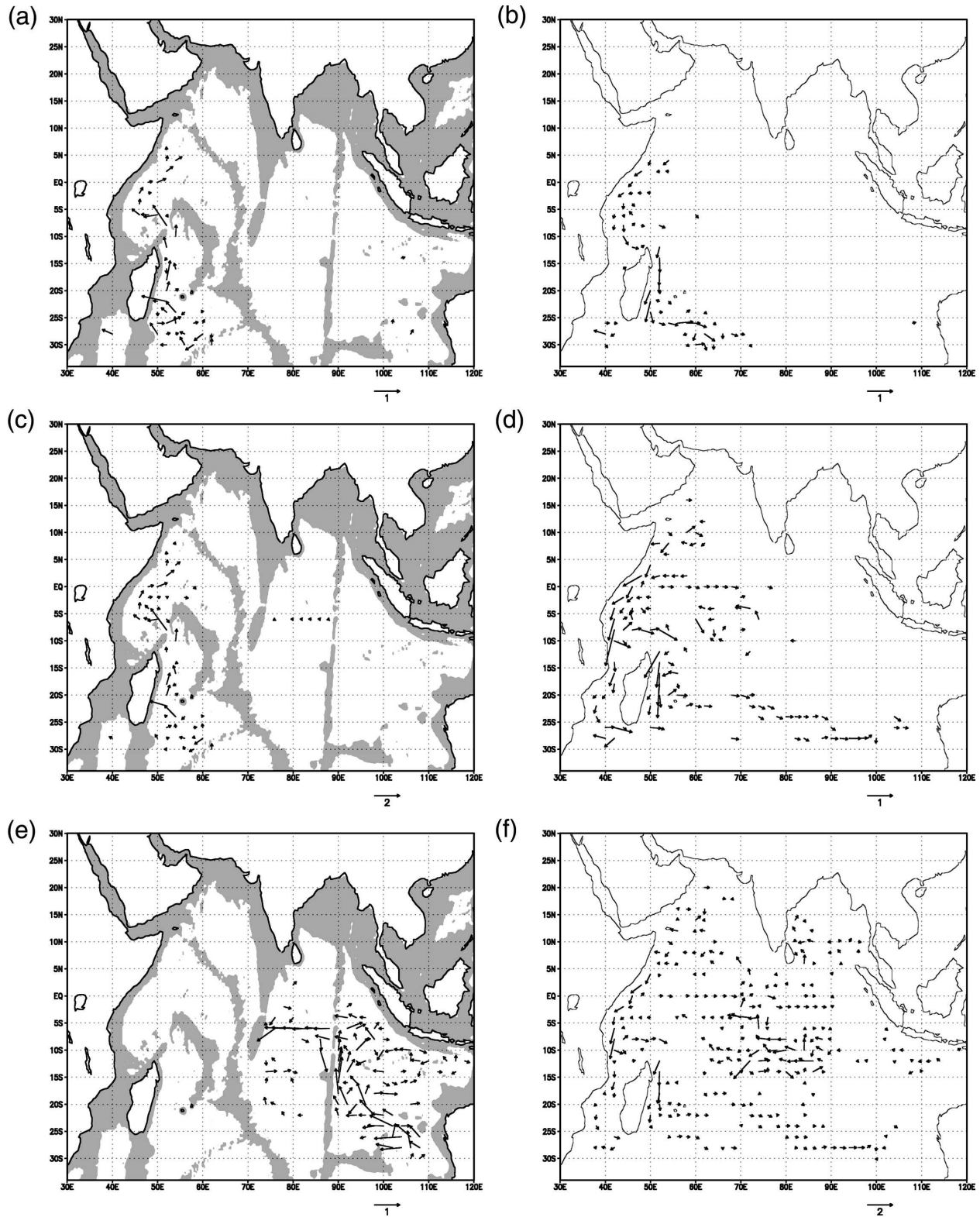
FIG. 10. (a) Vector plot of the Lagrangian transport associated with the deep inflow of the direct overturning. Vectors are plotted with a cutoff value of 0.01 Sv. The scaling is denoted below each plot. (b), (c) As in (a), but for (b) the deep outflow and (c) the indirect overturning with inflow from the west. The cutoff value is increased to 0.025 Sv. (d), (e) As in (c), but for (d) the deep outflow and (e) the indirect overturning with inflow from the east. (f) As in (e), but for the deep outflow.

cyclonic gyre in the Arabian Sea. At 20°S the outflow turns southeastward and connects the Madagascar and West Australian Basins.

The indirect overturning associated with the eastern inflow features the strongest transport into the West Australian Basin between 100° and 110°E, as observed by Sloyan (2006), and turns northwestward thereafter (Fig. 10e). North of 20°S the pathway proceeds in a northward jet along the eastern flank of the Ninetyeast Ridge. Then, in part, it recirculates cyclonically in the North Australian Basin, with another component crossing the ridge and forming a westward jet along 7°S that goes on to contribute to a deep cyclonic gyre occupying the southern half of the Central Indian Basin. The outflow branch of this overturning component exhibits a complex structure spanning a wide swath of the Indian Ocean. The most prominent outflow pathways are revealed by an eastward flow along the equator, an anticyclonic recirculation centered near the equator and around 80°E and, especially, a large cyclonic gyre in the subtropical Indian Ocean with outflow near 70° and 100°E across the southern boundary.

Summarizing, our diagnostics suggest that more water upwells to the west than to the east of its inflow site at the Indian Ocean's southern boundary. Further, the lower limb of the deep Indian Ocean overturning features predominantly westward flow, and the upper limb is mostly characterized by eastward flow. All of this evidence points toward the existence of a substantial depth-reversing zonal circulation in the deep Indian Ocean. This is illustrated most concisely by Fig. 11, which displays the (apparent) ZOC streamfunction. Note that the crossing of density surfaces by overturning streamlines is not necessarily associated with diaycnal upwelling or downwelling, but may also arise from inflow and outflow having different densities at any particular longitude. We now see in Fig. 11 that the depth-reversing zonal circulation in the deep Indian Ocean has an amplitude of 2.4 Sv, consistent with the decomposition in Table 1. The apparent upwelling branches near 50° and 70°E arise from actual diapycnal upwelling (see Fig. 7), whereas instead the apparent downwelling branches near 60° and 105°E are linked to large local inflow and outflow at different densities (Fig. 5b). At all longitudes, the meridionally averaged flow (not shown) is strongly westward in the deepest density classes, consistent with the streamfunction in Fig. 11. The only exception is found at 60°E, where the deep westward flow is largely blocked by the Central Indian Ridge. We also observe a lighter eastward return flow at all latitudes, distributed over a large interval in density space.

FIG. 11. The deep zonal overturning cell in the Indian Ocean as a function of neutral density and longitude. No attempt has been made to correct for the inflow and outflow across the southern boundary (30°S) of the domain. As a result, upwelling and downwelling branches can be associated with inflow and outflow occurring at different densities.

c. Implications for the ventilation of the deep Indian Ocean

The upshot of our diagnostics is that the existence of a substantial deep, depth-reversing zonal circulation of nearly 50% of the MOC, brought about by the zonally varying distribution of diapycnal mixing in the Indian Ocean, implies a much longer mean residence time for Indian Ocean deep waters than would be in place without the zonal circulation because of the extended advective pathway associated with the exchange between different zones. Close examination of Table 1 readily illustrates this point: the various components of the direct overturning circulation are associated with much shorter residence times than those of the indirect overturning circulation. This is substantiated by Fig. 12, which displays binned and accumulated volume transport as a function of travel time in the Indian Ocean for the direct (Fig. 12a) and indirect (Fig. 12b) components of the overturning circulation. Residence times for the indirect overturning circulation are approximately 5–6
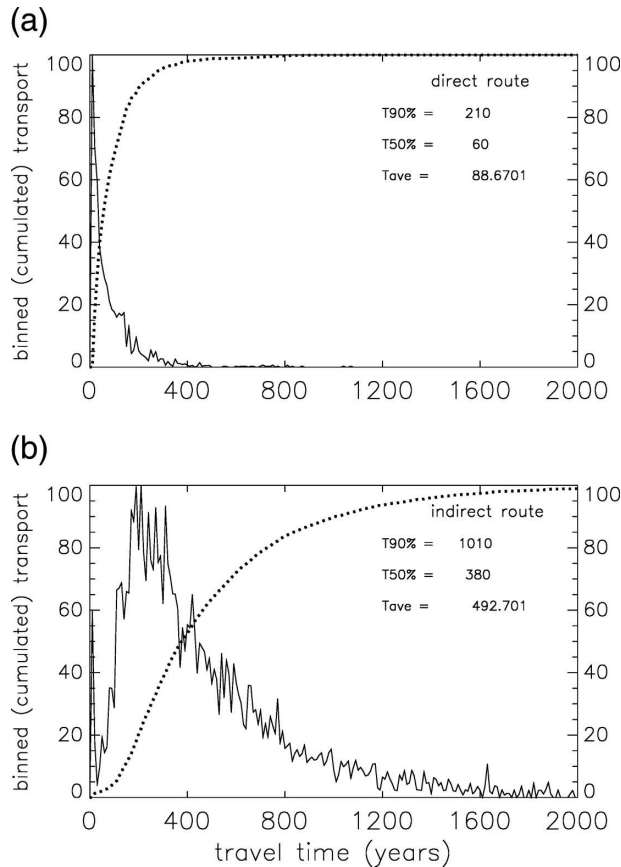
(a)

(b)

FIG. 12. Annually binned volume transport (dotted line) and time-integrated volume transport expressed as a percentage of the total transport (solid line) for the (a) direct and (b) indirect deep Indian Ocean overturning circulation. The annually binned transport scales with the maximum of the integration. Transport time scales are indicated on the upper-right-hand corner of each figure.

times longer than for the direct overturning circulation, with an average value of 90 (490) yr for the direct (indirect) overturning. It thus follows that the zonal asymmetry in the distribution of diapycnal mixing must have a major impact on the deep Indian Ocean's mean rate of ventilation and its capacity to store and transform physical and biogeochemical tracers.

5. Summary and concluding remarks

We have used a global eddy-permitting OGCM (OCCAM) to study the three-dimensional structure of the deep Indian Ocean MOC. Much as those parameterizations in other ocean models, the representation of diapycnal mixing in OCCAM is inaccurate and likely results in excessively low mixing rates in the deep Indian Ocean which are too weak to sustain a substantial overturning circulation indefinitely. Nonetheless, the

short model spinup prevents any considerable departure of the modeled density field from its initial climatological state, while permitting a realistic horizontal circulation to develop in a dynamically consistent manner. We have argued, using a Lagrangian technique, that the combination of these two circumstances offers a window of opportunity to study the effect of diapycnal mixing in the circulation of the real ocean, because the effective diapycnal velocity in the model (i.e., the sum of model drift and the modeled diapycnal velocity) bears some resemblance to the diapycnal velocity in the real ocean.

We note that these results have been obtained with time-independent velocity fields. It is well known that the deep circulation in the western Indian Ocean is characterized by large seasonal variability (Lee and Marotzke 1998; Beal et al. 2000). However, the impact of resolving this seasonal variability on our analysis of the OCCAM deep overturning circulation strength, pathways, and upwelling sites is small in spite of the model's deep flow field displaying significant seasonal changes, including sign reversals in some of the deep inflows and outflows. Further, we cannot discount the possibility that variability on the eddy time scale, which may induce chaotic advection and effectively enhance the stirring and mixing action of the flow (e.g., Drijfhout et al. 2003), may be a significant (although logistically unavoidable) omission from our analysis. The effect of such motion may very well increase the residence times shown in Table 1 and Fig. 12. Nonetheless, we have no reason to believe that the zonal asymmetry in diapycnal upwelling, the resulting existence of a zonal dimension to the deep Indian Ocean overturning circulation, and the relative differences in residence times for various routes seen in OCCAM should depend importantly on the inclusion of chaotic advection resulting from mesoscale eddy variability.

In illustration of our key point, we have demonstrated that OCCAM recovers the broad zonal asymmetry in the distribution of the turbulent buoyancy flux that is suggested by observations of oceanic fine structure, altimetric estimates of tidal energy dissipation (Egbert and Ray 2001), and the deep potential vorticity (McCarthy and Talley 1999) and radiocarbon (Srinivasan et al. 2000) fields. The amplitude of the deep MOC in the modeled Indian Ocean (5.6 Sv) is feasible in the context of global ocean circulation energetics (Wunsch and Ferrari 2004), albeit somewhat weaker than many observational estimates. In association with the zonally asymmetric deep overturning closure, the model features a substantial depth-reversing zonal circulation that amounts to approximately half of the MOC. The existence of a pronounced zonal dimension

to the deep Indian Ocean MOC implies a much longer residence time for Indian Ocean deep waters and a much-reduced rate of ventilation of the Indian Ocean abyss, which has important ramifications for the region's capacity in the storage and cycling of physical and biogeochemical substances. Indeed, we have shown that the component of the deep Indian Ocean MOC involving zonal (interbasin) exchanges is, on average, characterized by a residence time that is 5–6 times longer (490 yr) than that of the direct meridional overturning (90 yr). This long residence time may well play a key role in explaining the large nutrient and carbon enrichment and oxygen depletion undergone by the deep-water upwelling in the Indian Ocean (Srinivasan et al. 2000; Ganachaud and Wunsch 2002). These biogeochemical characteristics are subsequently and conspicuously imprinted on the Upper Circumpolar Deep Water of the Southern Ocean (Callahan 1972). Finally, the greatly extended transit path and residence time of water masses in the deep Indian Ocean associated with the overturning's zonal dimension imply that physical and biogeochemical anomalies introduced during ventilation in the North Atlantic and Southern Oceans will propagate upward at a decreased rate, tend to disperse in the zonal direction, and take a relatively long time to reemerge at the southern boundary of the Indian Ocean.

REFERENCES

Barton, E. D., and A. E. Hill, 1989: Abyssal flow through the Amirante Trench (western Indian Ocean). *Deep-Sea Res.,* **36,** 1121–1126.

Beal, L. M., R. L. Molinari, T. K. Chereskin, and P. E. Robbins, 2000: Reversing bottom circulation in the Somali Basin. *Geophys. Res. Lett.,* **27,** 2565–2568.

Becker, J. J., and D. T. Sandwell, cited 2004: SRTM30_PLUS: SRTM30, coastal and ridge multibeam, estimated topography. [Available online at http://topex.ucsd.edu/WWW_html/srtm30_plus.html.]

Blanke, B., and S. Raynaud, 1997: Kinematics of the Pacific Equatorial Undercurrent: An Eulerian and Lagrangian approach from GCM results. *J. Phys. Oceanogr.,* **27,** 1038–1053.

Broecker, W. S., 1991: The great ocean conveyor. *Oceanography,* **4,** 79–89.

Bryden, H. L., and L. M. Beal, 2001: Role of the Agulhas Current in Indian Ocean circulation and associated heat and freshwater fluxes. *Deep-Sea Res.,* **48,** 1821–1845.

Callahan, J. E., 1972: The structure and circulation of deep water in the Antarctic. *Deep-Sea Res.,* **19,** 563–575.

Dengler, M., and D. Quadfasel, 2002: Equatorial deep jets and abyssal mixing in the Indian Ocean. *J. Phys. Oceanogr.,* **32,** 1165–1180.

——, ——, F. Schott, and J. Fischer, 2002: Abyssal circulation in the Somali Basin. *Deep-Sea Res. II,* **49,** 1297–1322.

Döös, K., 1995: Interocean exchange of watermasses. *J. Geophys. Res.,* **100,** 13 499–13 514.

Drijfhout, S. S., P. de Vries, K. Döös, and A. C. Coward, 2003: Impact of eddy-induced transport on the Lagrangian structure of the upper branch of the thermohaline circulation. *J. Phys. Oceanogr.,* **33,** 2141–2155.

Egbert, G. D., and R. D. Ray, 2001: Estimates of M_2 tidal energy dissipation from TOPEX/POSEIDON altimeter data. *J. Geophys. Res.,* **106,** 22 475–22 502.

Ferron, B., and J. Marotzke, 2003: Impact of 4D-variational assimilation of WOCE hydrography on the meridional circulation of the Indian Ocean. *Deep-Sea Res.,* **50,** 2005–2021.

Fieux, M., and J. C. Swallow, 1988: Flow of deep water into the Somali Basin. *Deep-Sea Res.,* **35,** 303–309.

Ganachaud, A., and C. Wunsch, 2000: Improved estimates of global ocean circulation, heat transport and mixing from hydrographic data. *Nature,* **408,** 453–457.

——, and ——, 2002: Oceanic nutrient and oxygen transports and bounds on export production during the World Ocean Circulation Experiment. *Global Biogeochem. Cycles,* **16,** 1057, doi:10.1029/2000GB001333.

——, ——, J. Marotzke, and J. Toole, 2000: Meridional overturning and large-scale circulation of the Indian Ocean. *J. Geophys. Res.,* **105,** 26 117–26 134.

Garternicht, U., and F. Schott, 1997: Heat fluxes of the Indian Ocean from a global eddy-resolving model. *J. Geophys. Res.,* **102,** 21 147–21 159.

Gibson, R., P. Kallberg, S. Uppala, A. Hernández, A. Nomura, and E. Serrano, 1997: The ERA description. ECMWF Re-Analysis Project Report Series 1, 71 pp.

Jackett, D. R., and T. J. McDougall, 1997: A neutral density variable for the world's oceans. *J. Phys. Oceanogr.,* **27,** 237–264.

Johnson, G. C., B. A. Warren, and D. B. Olson, 1991: Flow of bottom water in the Somali Basin. *Deep-Sea Res.,* **38,** 637–652.

——, D. L. Musgrave, B. A. Warren, A. Ffield, and D. B. Olson, 1998: Flow of bottom and deep water in the Amirante Trench and Mascarene Basin. *J. Geophys. Res.,* **103,** 30 973–30 984.

Kobayashi, T., and T. Suga, 2006: The Indian Ocean HydroBase: A high-quality climatological dataset for the Indian Ocean. *Prog. Oceanogr.,* **68,** 75–114.

Kunze, E., E. Firing, J. M. Hummon, T. K. Chereskin, and A. Thurnherr, 2006: Global abyssal mixing inferred from lowered ADCP shear and CTD strain profiles. *J. Phys. Oceanogr.,* **36,** 1553–1576.

Lee, M.-M., A. C. Coward, and A. J. G. Nurser, 2002: Spurious diapycnal mixing of the deep waters in an eddy-permitting global ocean model. *J. Phys. Oceanogr.,* **32,** 1522–1535.

Lee, T., and J. Marotzke, 1997: Inferring meridional mass and heat transports in the Indian Ocean by combining a general circulation model with climatological data. *J. Geophys. Res.,* **102,** 10 585–10 602.

——, and ——, 1998: Seasonal cycles of meridional overturning and heat transport of the Indian Ocean. *J. Phys. Oceanogr.,* **28,** 923–943.

Levitus, S., and T. P. Boyer, 1994: *Temperature*. Vol. 4, *World Ocean Atlas 1994,* NOAA Atlas NESDIS 4, 117 pp.

——, R. Burgett, and T. P. Boyer, 1994: *Salinity*. Vol. 3, *World Ocean Atlas 1994,* NOAA Atlas NESDIS 3, 99 pp.

Lumpkin, R., and K. Speer, 2007: Global ocean meridional overturning. *J. Phys. Oceanogr., 37,* 2550–2562.

Luyten, J. R., and J. C. Swallow, 1976: Equatorial undercurrents. *Deep-Sea Res., 23,* 999–1001.

Macdonald, A., 1998: The global ocean circulation: A hydrographic estimate and regional analysis. *Prog. Oceanogr., 41,* 281–382.

Mantyla, A. W., and J. L. Reid, 1995: On the origins of deep and bottom waters of the Indian Ocean. *J. Geophys. Res., 100,* 2417–2439.

McCarthy, M. C., and L. D. Talley, 1999: Three-dimensional isoneutral potential vorticity structure in the Indian Ocean. *J. Geophys. Res., 104,* 13 251–13 267.

——, ——, and M. O. Baringer, 1997: Deep upwelling and diffusivity in the southern Central Indian Basin. *Geophys. Res. Lett., 24,* 2801–2804.

Naveira Garabato, A. C., H. Bryden, and E. McDonagh, 2005: Closing the meridional overturning circulation of the Indian Ocean: The mixing perspective. *Geophysical Research Abstracts,* Vol. 7, Abstract 05052.

Palmer, M. D., A. C. Naveira Garabato, J. D. Stark, J. Hirschi, and J. Marotzke, 2007: The influence of diapycnal mixing on quasi-steady overturning circulation states in the Indian Ocean. *J. Phys. Oceanogr., 37,* 2290–2304.

Polzin, K. L., J. M. Toole, J. R. Ledwell, and R. W. Schmitt, 1997: Spatial variability of turbulent mixing in the abyssal ocean. *Science, 276,* 93–96.

Ponte, R. M., and J. R. Luyten, 1990: Deep velocity measurements in the western equatorial Indian Ocean. *J. Phys. Oceanogr., 20,* 43–52.

Quadfasel, D., J. Fischer, F. Schott, and L. Stramma, 1997: Deep water exchange through the Owens Fracture Zone in the Arabian Sea. *Geophys. Res. Lett., 24,* 2805–2808.

Reid, J. L., 2003: On the total geostrophic circulation of the Indian Ocean: Flow patterns, tracers and transports. *Prog. Oceanogr., 56,* 137–186.

Robbins, P. E., and J. M. Toole, 1997: The dissolved silica budget as a constraint on the meridional overturning circulation of the Indian Ocean. *Deep-Sea Res., 44,* 879–906.

Saunders, P. M., A. C. Coward, and B. A. de Cuevas, 1999: Circulation in the Pacific Ocean seen in a global ocean model: Ocean Circulation and Climate Advanced Modelling project (OCCAM). *J. Geophys. Res., 104,* 18 281–18 300.

Schmitz, W. J., Jr., 1995: On the interbasin-scale thermohaline circulation. *Rev. Geophys., 33,* 151–173.

Sloyan, B. M., 2006: Antarctic bottom and lower circumpolar deep water circulation in the eastern Indian Ocean. *J. Geophys. Res., 111,* C02006, doi:10.1029/2005JC003011.

——, and S. R. Rintoul, 2001: The Southern Ocean limb of the global deep overturning circulation. *J. Phys. Oceanogr., 31,* 143–173.

Srinivasan, A., C. G. H. Rooth, Z. Top, and D. B. Olson, 2000: Abyssal upwelling in the Indian Ocean: Radiocarbon diagnostics. *J. Mar. Res., 58,* 755–778.

——, Z. Top, P. Schlosser, R. Hohmann, M. Iskandarani, D. B. Olson, J. E. Lupton, and W. J. Jenkins, 2004: Mantle ^3He distribution and deep circulation in the Indian Ocean. *J. Geophys. Res., 109,* C06012, doi:10.1029/2003JC002028.

Talley, L. D., J. L. Reid, and P. E. Robbins, 2003: Data-based meridional overturning streamfunctions for the global ocean. *J. Climate, 16,* 3213–3226.

Thurnherr, A. M., 2006: Diapycnal mixing associated with an overflow in a deep submarine canyon. *Deep-Sea Res., 53,* 194–206.

Toole, J. M., and B. A. Warren, 1993: A hydrographic section across the subtropical South Indian Ocean. *Deep-Sea Res., 40,* 1973–2019.

Warren, B. A., 1981: Transindian hydrographic section at Lat. 18S: Property distributions and circulation in the South Indian Ocean. *Deep-Sea Res., 28,* 759–788.

——, 1982: The deep water of the central Indian Basin. *J. Mar. Res., 40* (Suppl.), 823–860.

——, and G. C. Johnson, 2002: The overflows across the Ninetyeast Ridge. *Deep-Sea Res. II, 49,* 1423–1439.

Webb, D. J., A. C. Coward, B. A. de Cuevas, and C. S. Gwilliam, 1997: A multiprocessor ocean general circulation model using message passing. *J. Atmos. Oceanic Technol., 14,* 175–183.

Wunsch, C., and R. Ferrari, 2004: Vertical mixing, energy, and the general circulation of the oceans. *Annu. Rev. Fluid Mech., 36,* 281–314.

Zhang, Q., and J. Marotzke, 1999: The importance of open boundary estimation for an Indian Ocean GCM-data synthesis. *J. Mar. Res., 57,* 305–334.